The Journal of Supercritical Fluids 135 (2018) 168–179

Contents lists available at ScienceDirect

The Journal of Supercritical Fluids

journal homepage: www.elsevier.com/locate/supflu

Rate-based simulation of a high pressure counter-current packed column for supercritical CO_2 extraction of alcohol from dilute aqueous mixtures

Nicolás Gañán[a,b], Jérôme Morchain[b], Séverine Camy[c,*], Jean-Stéphane Condoret[c]

[a] Instituto de Investigación y Desarrollo en Ingeniería de Procesos y Química Aplicada (IPQA), Universidad Nacional de Córdoba, CONICET, Av. Vélez Sarsfield 1611, X5016GCA, Córdoba, Argentina
[b] LISBP, Université de Toulouse, CNRS, INRA, INSA, Toulouse, France
[c] Laboratoire de Génie Chimique, Université de Toulouse, CNRS, INPT, UPS, Toulouse, France

GRAPHICAL ABSTRACT

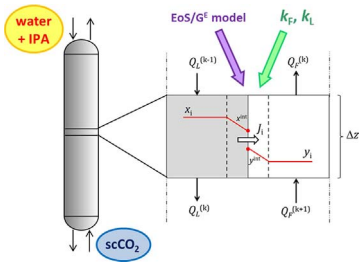

ARTICLE INFO

Keywords:
Supercritical CO_2 extraction
Packed column
Mass transfer
Rate-based modeling
Isopropanol

ABSTRACT

In this work, the modeling and simulation of a fractionation packed column for the recovery of isopropanol from dilute aqueous mixtures using supercritical CO_2 is presented. The model is based on the numerical resolution of differential mass balances for each component over the column height. The multicomponent mass transfer between phases is described using a "rate-based" approach and the concept of local mass transfer coefficients. The model was validated by reproduction of experimental steady-state results for the fractionation of 5% isopropanol aqueous solutions obtained in a bench scale counter-current column. The effect of process conditions on the separation performance was satisfactorily described by the model calculations, showing that operation pressure and CO_2 flow rate enhance IPA recovery and extract purity, while operation temperature has a negative effect. Model deviations (AARD) were in all cases lower than 20%.

1. Introduction

Fractionation of liquid mixtures using supercritical solvents has been proposed and studied as a promising tool for new separation challenges, as well as an alternative to current separation processes [1,2]. In this way, the use of supercritical carbon dioxide ($scCO_2$) as a solvent proposes a more environmentally friendly technology when compared to conventional organic solvents. The main potential applications include deterpenation of citrus oils [3–6], purification and removal of solvent residues from edible oils [7], fractionation of fish oils [8,9], recovery of high value lipid compounds from edible oils or by-products [10,11] and extraction of alcohols and other organic solvents from aqueous solutions [12,13].

In a typical fractionation process, the mixture to be separated and the supercritical solvent are fed to a separation column (generally a packed column) operated in counter-current mode. During contact, the components of the mixture distribute between the liquid and supercritical phases according to their volatility and affinity for $scCO_2$ to an

* Corresponding author.
E-mail address: severine.camy@ensiacet.fr (S. Camy).

https://doi.org/10.1016/j.supflu.2018.01.020
Received 6 November 2017; Received in revised form 21 January 2018; Accepted 22 January 2018

Nomenclature

a_{eff}	Effective interfacial area [m^2/m^3]
a_p	Packing specific surface area [m^2/m^3]
D_{ij}	Binary diffusion coefficient of components i and j [m^2/s]
d_p	Packing characteristic dimension [m]
g	Gravity acceleration [m/s^2]
Ga	Galilei number $Ga = g{d_p}^3{\rho_L}^2/{\mu_L}^2$
h_L	Volumetric liquid hold up (volume of liquid/internal column volume)
J_i	Interfacial mass transfer flux of component i [kg/m^2 s]
$k_{i,F}$	Fluid phase local mass transfer coefficient [m/s]
$k_{i,L}$	Liquid phase local mass transfer coefficient [m/s]
m_i	Partition coefficient of component i
N	Number of discretisation elements in the column
NC	Number of components
Q	Mass flow rate [kg/s]
Re	Reynolds number
S	Column section area [m^2]
Sc	Schmidt number $Sc = \mu/(\rho D)$
u	Superficial velocity [m/s]
We	Weber number $We = d_p{Q_L}^2/(S^2\rho_L\sigma_L)$
x_i	Mass fraction of component i in the liquid phase
y_i	Mass fraction of component i in the fluid phase
z	Height [m]
ε	Packing void fraction
μ_F	Fluid phase viscosity [Pa s]
μ_L	Liquid phase viscosity [Pa s]
ρ_F	Fluid phase density [kg/m^3]
ρ_L	Liquid phase density [kg/m^3]
σ_c	Critical surface tension of packing material [N/m]
σ_L	Liquid phase surface tension [N/m]

extent determined by the prevailing temperature, pressure and composition conditions, as well as the effective mixing and contact area of the phases. The supercritical phase leaving the column at the top ("extract") is then totally or partially expanded in a separator where solutes condense and are recovered. The processed liquid phase leaves the column at the bottom ("raffinate"). The general features of this process are similar to the gas-liquid contacting operations, and therefore its mathematical description is usually analogous or directly based on the theories developed for those operations. The main differences are connected to the particular properties of the supercritical phase (which cannot be considered simply as a gas, because of its significantly higher density and viscosity) together with the complexities of high pressure phase equilibria in ternary or multicomponent systems.

Due to the usually large solvent flow rates required by such processes when CO_2 is used, process optimization is fundamental to assess economic feasibility, including not only the fractionation column but also the separators and solvent regeneration cycle. Costly and time-consuming experimental work [14] can be alleviated through the use of computational tools based on robust and reliable thermodynamic and mass transfer models.

Similarly to gas-liquid and liquid-liquid operations, two different approaches can be proposed for modeling and simulation of supercritical fractionation columns: (*i*) methods based on the concept of equilibrium stage, and (*ii*) rate-based or "non-equilibrium" methods, based upon hydrodynamic and interfacial mass transfer along with a thermodynamic equilibrium assumption at the interface.

In "equilibrium stage" methods the column is modeled as a succession of discrete units where the phases mix and reach equilibrium before separating. Concentrations are assumed to be homogeneous in each phase. This approach is applied to packed columns through the concept of "height equivalent to a theoretical stage" (HETS), i.e., the height of packed bed which produces a separation output similar to an equilibrium stage. Many commercial process simulation softwares propose calculation modules for contactors based on this approach. Although easy to implement and very useful to assess and compare performances of a complete process, equilibrium stage methods are somewhat limited due to the poor generalization capability of the concept of HETS or "stage efficiency", which is very dependent on the physical properties of the system and the flow rates, as well as the contacting technology. Therefore their evaluation is complex and highly sensitive to the operating conditions.

On the other hand, rate-based methods take into account the mass transfer kinetics between phases and do not assume that the phases are globally in equilibrium after contact but only at the interface. For this reason, they are often called "non-equilibrium" methods. In these models, the mass transfer and hydrodynamic particularities of each system are explicitly computed based on physical and geometrical properties. Ruivo et al. [15] applied this approach to the dynamic simulation of the separation of methyl oleate and squalene with $scCO_2$ in a counter-current structured packing column. Their model consists in a set of differential mass balances for each phase and algebraic equations accounting for mass transfer and hydrodynamic aspects. Phase equilibrium at the interface was taken into account through an empirical correlation, and the interfacial fluxes were calculated using overall mass transfer coefficients. With this model, steady state but also the initial transient period and the dynamic response to perturbations could be described. In a more recent work, Fernandes et al. [16] have extended this model to non-isothermal operation by incorporating an energy balance. Martin and Cocero [17] have developed a steady state model for the $scCO_2$ fractionation of liquid mixtures in counter-current packed columns with external reflux based on differential mass and energy balances, describing mass transfer by Maxwell-Stefan multicomponent diffusion theory. Their model was validated against experimental data on edible oils fractionation and fish oil ethyl esters separation. The model was solved by an iterative method, guessing the outlet gas flow rate and composition and calculating backwards the corresponding inlet values until obtaining the specified or experimental values within a certain tolerance. The only fitted parameter was the effective interfacial area.

In the present work, a dynamic rate-based model of a high-pressure counter-current packed column is presented and applied to the simulation of the extraction of isopropanol (IPA) from dilute aqueous solutions using $scCO_2$. This kind of separations is of great interest for the recovery of bio-alcohols in fermentation processes, and has been experimentally studied in bench scale fractionation column in our previous work [18]. Two different types of packing and various operating conditions have been studied. In that work, the fractionation process was described using the equilibrium stage approach. The number of equilibrium stages was found to be between one and two for a 2 m height column, this number being dependent on operating conditions, which reflects the fact that the stage approach is not well suited to that particular case. The same ternary system has been previously studied by Rathkamp et al. [19] who characterized mass transfer performances of a spray column, with and without a packing, and proposed a description using the conventional NTU-HTU approach. In their work they considered droplets of fluid phase flowing through a continuous liquid phase, with transfer of isopropanol only, and described thermodynamics using a constant partition coefficient, which is likely to be not enough accurate for these complex systems. We propose here to further analyse our previous experimental results making use of a dynamic rate-based model. In order to preserve the numerical cost at a reasonable expense, the thermodynamic equilibrium data over a large range of operating conditions are calculated first and embedded in the dynamic simulator as correlations. With this approach, the concentration profiles

in both phases and the mass transfer resistance of both phases are accurately and quickly computed, yielding to a better understanding of physical and thermodynamic phenomena. In particular, it allows identifying a possible mass transfer limitation by one of the phases, giving some guidance for technological improvement.

2. Model formulation

2.1. Model equations

Fig. 1 shows a schematic representation of the fractionation column with the different streams entering and leaving the column, as well as a simplified picture of the interfacial mass transfer process for a differential volume of height Δz. The liquid feed entering at the top is a dilute aqueous solution of isopropanol (IPA, 5% wt.) while the solvent feed at the bottom consists in pure $scCO_2$.

The mathematical model is based on a set of differential mass balance equations for each component in each phase, and a set of algebraic equations and correlations accounting for phase equilibria and mass transfer phenomena. The mass balance equations for a component i over a differential volume, Sdz, of the packed bed are given in Eqs. (1) and (2):

$$\frac{\partial(\varepsilon h_L \rho_L x_i)}{\partial t} = -\frac{1}{S}\frac{\partial(Q_L x_i)}{\partial z} - a_{\text{eff}} J_i \quad \text{for } i = 1...NC \quad \text{(liquid phase)} \tag{1}$$

$$\frac{\partial[\varepsilon(1-h_L)\rho_F y_i]}{\partial t} = -\frac{1}{S}\frac{\partial(Q_F y_i)}{\partial z} + a_{\text{eff}} J_i \quad \text{for } i = 1...NC \quad \text{(supercritical fluid phase)} \tag{2}$$

where S is the cross section of the column, z is the axial coordinate, ε is the dry packing void fraction, h_L is the liquid volumetric fraction or hold-up, a_{eff} is the effective interfacial area per unit volume and J_i is the interfacial mass transfer flux of each species. NC is the number of components ($NC = 3$ in our case, 1 = IPA, 2 = water, 3 = CO_2), Q_L and Q_F are the total mass flow rates of the aqueous solution (referred as "liquid") and the supercritical CO_2 phase ("fluid") respectively and finally x_i, y_i are the mass fractions of the component i in the bulk of the liquid and fluid phases, respectively.

The column was assumed to operate at constant temperature and therefore thermal effects are not considered. Axial dispersion in both phases is not taken into account in our model. Indeed, this phenomenon is probably negligible due to the high value of the ratio height of the column/size of the packing.

From the double resistance approach, the interfacial mass transfer fluxes (of water and IPA from the liquid to the fluid phase and of CO_2 from the fluid to the liquid phase) were expressed in terms of local mass transfer coefficients, according to Eq. (3):

$$J_i = k_{i,F}\rho_F(y_i^{\text{int}} - y_i) = -k_{i,L}\rho_L(x_i^{\text{int}} - x_i) \tag{3}$$

The interfacial mass fractions of IPA (x^{int} and y^{int}) are determined by solving simultaneously the continuity of fluxes at the interface and the thermodynamic equilibrium relationships. The mass transfer coefficients of IPA and water in the fluid phase ($k_{1,\text{F}}$ and $k_{2,\text{F}}$) and IPA and CO_2 in the liquid phase ($k_{1,\text{L}}$ and $k_{3,\text{L}}$) were estimated using conventional correlations reported by Onda et al. for randomly packed columns [20,21] (Eqs. (4) and (4)). Because of the high density of supercritical CO_2, hydrodynamics in fluid-liquid contactors can be regarded as intermediate between gas/liquid and liquid/liquid behaviour. Indeed, it has been chosen in this study to assume that hydrodynamics in the packed column is of the gas-liquid type, with a liquid film flowing at the packing surface, on a similar way as gas absorption columns. This was also done for instance by Simoes et al. [22] for mass transfer coefficients estimation and by Stockfleth and Brunner [23] when dealing with hydrodynamics of supercritical packed columns.

$$k_{i,F} = \alpha\left[(a_p d_p)^{-2} Re_F^{0.7} Sc_F^{0.33}\left(\frac{D_{i3}}{d_p}\right)\right] \quad \text{for } i = 1, 2 \tag{4}$$

$$k_{i,L} = \beta\left[(a_p d_p)^{0.4} Re_L^{0.66} Sc_L^{-0.5}\left(\frac{\mu_L g}{\rho_L}\right)^{0.33}\right] \quad \text{for } i = 1, 3 \tag{5}$$

In these correlations, a_p and d_p are the specific surface area and the characteristic dimension of the packing respectively, D_{13} is the binary diffusivity of IPA in $scCO_2$, and Re and Sc are the Reynolds and Schmidt numbers, respectively. In order to take into account the possible lack of precision (Simoes et al. [22], Woerlee [24]) of the Onda conventional correlations in the case of high pressure system, we decided to replace original coefficients (obtained at atmospheric pressure) equal to 5.23 and 0.0051, respectively by α and β coefficients, which values are adjusted from experimental results.

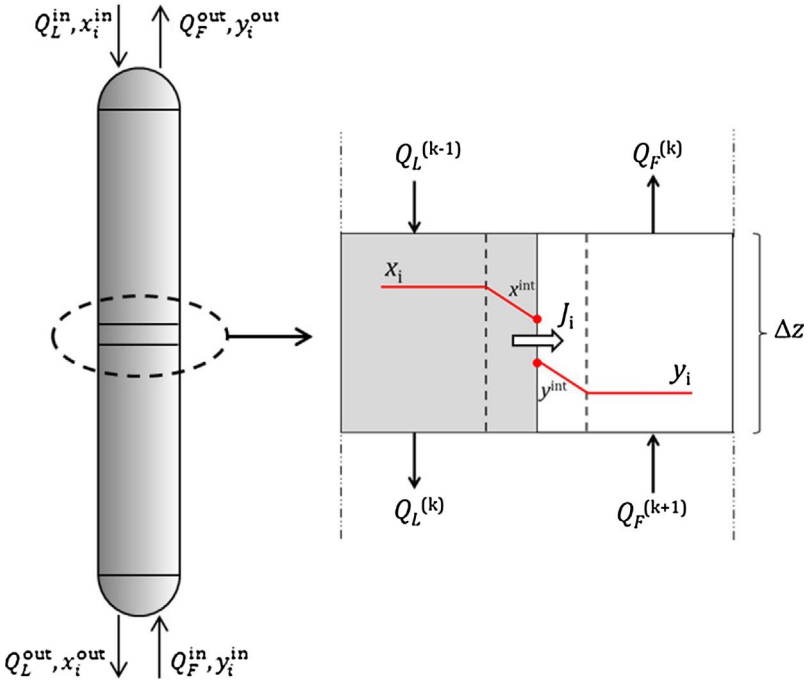

Fig. 1. Schematic representation of the fractionation column and the "double resistance" approach over a unit volume of packed bed (F: supercritical fluid phase, L: liquid phase).

Note that the Reynolds number for the liquid phase has to be calculated in terms of effective interfacial area (a_{eff}), as in Eq. (6):

$$Re_L = \frac{Q_L}{Sa_{\text{eff}}\mu_L} \tag{6}$$

The effective interfacial area was assumed to be equal to the wetted packing area, which was estimated with the following correlation from Onda et al. (Eq. (7)):

$$\frac{a_{\text{eff}}}{a_p} = 1 - \exp\left[-1.45\left(\frac{\sigma_c}{\sigma_L}\right)^{0.75}(a_p d_p)^{0.35} Ga_L^{0.05} We_L^{0.2}\right] \tag{7}$$

where σ_c is the "critical" surface tension of the packing material and σ_L the surface tension of the liquid. Ga_L and We_L are the Galilei and Weber numbers for the liquid phase, respectively. The calculation of themodynamical and physico-chemical properties is presented in the following sections.

Finally, the liquid hold up (h_L) was estimated with a standard correlation for randomly packed columns [25], according to Eq. (9):

$$h_L = 1.295(a_p d_p) Ga_L^{-0.44} Re_L^{0.676} \tag{8}$$

All symbols and non-dimensional numbers are defined in the nomenclature. All details regarding the characteristics of the fractionation column can be found in our previous work [18]. The main information is reported in Table 2.

2.2. Thermodynamic model

As mentioned, the model assumes thermodynamic equilibrium at the interface. The IPA-water-CO_2 ternary phase equilibrium was computed using the Simulis® Thermodynamics software (ProSim SA, France). A combined equation of state/activity coefficient model (EoS/G^E) approach with suitable complex mixing rules was selected. The equation of state is the Soave-Redlich-Kwong equation [26] with the modification proposed by Boston-Mathias [27]. The co-volume b of the SRK equation is obtained from a standard mixing rule (arithmetic mean of the corresponding parameters of the pure compounds). The term a of the SRK equation is computed using the PSRK mixing rule [28] and the UNIQUAC model [29,30] is used to calculate the excess energy at zero pressure, G_0^E, involved in the PSRK mixing rule. More detailed information about the modeling of the system phase behaviour can be found in our previous work [18].

2.3. Physico-chemical properties

The equations involved in the column model require the knowledge or an estimation of several physico-chemical properties of the pure compounds. The needed physico-chemical properties of pure IPA, water and CO_2 are presented in Table 1, as obtained from NIST.

The density and viscosity of the fluid and liquid phases were assumed to be constant along the column and equal to those of pure CO_2 and pure water at the specified pressure and temperature conditions, neglecting the effect of the low concentration of solutes and the composition changes along the column. This simplification, limited to dilute liquid solutions, was verified with available experimental data.

For density of the liquid phase, experimental results reported by Hebach et al. [31] indicate that the density of CO_2-saturated water within the range of operation conditions covered in this work differs only around 1% with respect to pure water at the same conditions. Regarding the fluid phase, to the best of our knowledge there are no density data for the systems CO_2 + water or CO_2 + isopropanol at supercritical conditions in the open literature. However, as a reference, data of saturated density of the system CO_2 + ethanol at near critical and supercritical conditions (40 and 55 °C, 7–9 MPa) indicate that the difference with pure CO_2 density is below 12% [32]. Calculations performed with the Simulis© software using our thermodynamic model for a mixture consisting in 99% CO_2, 0.5% water and 0.5% IPA (close to the composition of the fluid phase in the column) predict a 9% deviation with respect to pure CO_2 density, as provided by the NIST data base.

Supercritical fluid phase viscosity was estimated with the method of Lucas [33] for dilute mixtures of IPA and water (up to 2%) in scCO_2 and was found similar to the viscosity of pure CO_2 under the same conditions within a maximum deviation range of 15%. For the viscosity of the liquid phase, data reported by Tanaka et al. [34] show that the viscosity of aqueous solutions of IPA under pressure increases with IPA concentration, reaching a maximum at around 60% wt. On the other hand, it is known that the dissolution of supercritical solvents in liquids decreases their viscosity. For example, data of CO_2 + oleic acid and CO_2 + squalene show that the saturated liquid viscosity is reduced with increasing pressure, along with a higher dissolution of CO_2 [35]. To the best of our knowledge, there is no information regarding the viscosity of water saturated with CO_2 at high pressure conditions, but a similar behaviour is expected to occur, although in a lesser extent considering that scCO_2 solubility in water is lower than in lipidic liquids. Therefore, considering the opposite effects of IPA and CO_2 on the aqueous phase viscosity, the latter was assumed to be equal to that of pure water.

The surface tension of the liquid phase (σ_L) was estimated using the method of Tamura, recommended for aqueous solutions of organic compounds [33], corrected to account for the effect of pressure. The details of this method are given in Appendix A. Briefly, the mixture surface tension is calculated by interpolation of the pure compound values as a function of the mixture composition. The model was fitted to experimental data of surface tension for the ternary system IPA + water + CO_2 at high pressure conditions [36], and allowed estimation of the surface tension variation along the column. This was thought to be necessary due to the fact that this property is sensitive to the presence of IPA and has a strong influence on the value of the wetted or effective interfacial area, a key parameter for mass transfer.

The diffusion coefficients of IPA and water in the supercritical phase (D_{13} and D_{23}) and of IPA and CO_2 in the liquid phase (D_{12} and D_{32}) were estimated using the conventional method of Wilke and Chang [33] for liquids. The calculation details are given in Appendix B. Although this method provides an estimation of binary diffusion coefficients at infinite dilution, the values obtained are expected to hold because of the low concentration conditions that prevail in both phases in the case of dilute mixtures fractionation.

2.4. Numerical resolution

The model was implemented in the Matlab© software. The differential mass balance equations (Eqs. (1) and (2)) were solved using a finite difference discretization method based on N grid nodes. The first and last nodes receive the conventional following boundary conditions:

- at the inlet: flow rate and composition are constant
- at the outlet: zero gradient for all quantities.

A second order upwind scheme is used for internal nodes ($k = 3, \ldots, N-1$) as well as for the definition of the Neumann boundary

Table 1
Physico-chemical properties of pure compounds (from NIST[a]).

Property	IPA	water	CO_2
Molar mass (g/mol)	60	18	44
Critical temperature (°C)	235.9	373.6	31.1
Critical pressure (MPa)	4.9	22.1	7.38
Critical volume (cm^3/mol)	222.0	55.9	91.9
Molar volume at normal boiling point (cm^3/mol)	77	18	–

NIST webbook of chemistry http://webbook.nist.gov/chemistry/.
[a] National Institute of Standards and Technology.

condition at node N, according to Eq. (9):

$$\left.\frac{\partial(Q_L x_i)}{\partial z}\right|_k = \frac{3(Q_L x_i)_k - 4(Q_L x_i)_{k-1} + (Q_L x_i)_{k-2}}{2\Delta z} + O(\Delta z^2) \quad (9)$$

A second order centred scheme is used for the second node ($k = 2$), according to Eq. (10).

$$\left.\frac{\partial(Q_L x_i)}{\partial z}\right|_k = \frac{(Q_L x_i)_{k+1} - (Q_L x_i)_{k-1}}{2\Delta z} + O(\Delta z^2) \quad (10)$$

In this way, the set of 6 partial differential equations (3 components and 2 phases) is transformed into a set of $6N$ ordinary differential equations. The resulting system of ordinary differential equations and algebraic equations is integrated over time using a fourth order explicit Runge-Kutta (RK4) method. For each set of operating conditions, the time step is automatically adjusted in order to meet the stability criterion (current number < 1).

In general, concentrations as well as total and partial flow rates are function of time and location along the column. When the solution to be purified is concentrated, the solute extraction by $scCO_2$ may modify significantly the liquid flow rate (and all associated properties). Also, the dissolution of CO_2 in the liquid phase may be important in some cases, and therefore the fluid flow rate can be reduced in the same way. However, as previously mentioned, we consider in the present work dilute liquid feeds so it is acceptable to consider that the flow rates and the liquid hold-up are practically constant along the column. Therefore the resolution of the mass balance equations is simplified: for each time step they are solved considering constant h_L, Q_L and Q_F along the column, and only the initial composition profile of each phase is required as initial condition. This assumption holds as long as the net mass flux through the interface is small as compared to the mass flow rate of each phase. This clearly constitutes a limitation of our modeling approach which is indeed only valid for dilute mixtures but actually corresponds to the recovery of dilute alcohols from fermentation broths.

Solving this set of equations requires the calculation of the equilibrium concentrations at the interface for each node at each time step. Implementing these thermodynamic equilibrium calculations using Simulis© proved to yield very lengthy computations because of the numerous calls to an external procedure (i.e., the Simulis© software toolboxes). To improve the computational efficiency of this dynamic simulator, ternary equilibrium data were beforehand computed for a wide range of compositions, at the specified operation temperature and pressure, and stored as a set of cubic spline interpolation functions.

3. Results and discussion

3.1. Simulation parameters and preliminary runs

As mentioned, the model was validated by fitting experimental steady state fractionation data of dilute aqueous mixtures of IPA using $scCO_2$, obtained by Lalam et al. using a bench scale counter-current column, as reported in a previous work [18]. The adjustable coefficients of Eqs. (4) and (5) were obtained in order to reproduce the recovery ratio and mass fraction of IPA in the raffinate stream under different temperature, pressure and solvent-to-feed ratio conditions.

Table 2 shows the column and packing characteristics used in the experiments, required by the model as input information. Two types of packing have been evaluated: stainless steel springs and a porous metallic (FeCrAlY) foam.

A first set of preliminary runs were performed in order to determine appropriate discretization and integration parameters. In order to obtain reproducible and stable numerical results, 100 grid points (each of 2 cm height) and a time integration step of 0.3 s were sufficient in most cases. Calculations were carried out until the outlet concentrations were constant (steady state conditions). However, the accurate prediction of the transient period duration was not an objective of this work. The dynamic simulation approach is used here as a strategy to avoid the initialization problem that usually arises in steady state models, which are solved iteratively and whose performance rely on the quality of the initial guess of the outlet conditions [17].

As mentioned, due to the constant flow rate hypothesis, only the initial composition profiles along the column are required as initial conditions. Different initialization strategies were tested. The fluid phase was considered initially as pure $scCO_2$ in all runs, but different initial profiles for the liquid phase were tested: (*i*) pure water; (*ii*) a composition profile equal to that of the liquid feed, and (*iii*) variable composition profile with a linear gradient of IPA from the liquid feed composition at the top to zero at the bottom. In all cases, the model proved to converge toward the same steady state solution, with differences regarding the duration and behaviour of the transient period, as shown in Fig. 2 for a given set of operating conditions. Notice that the curves corresponding to the initial liquid phase configurations (*ii*) and (*iii*) almost completely overlap.

The model also provides information about the calculated concentration profiles along the column, as well as the interfacial mass transfer fluxes and partial flow rates. As an example, Fig. 3 shows the calculated profiles for the fractionation of a 5% IPA solution at 40 °C, 10 MPa and a solvent-to-feed ratio (Q_F/Q_L) equal to 9.5 kg/kg using the springs packing. This kind of information can be very useful for technological improvement, as it allows detecting if the mass transfer is low in a certain part of the column. It can be checked that the magnitude of the mass flux between phases remains small compared to the mass flux of each phase (total liquid mass flux is equal to 0.587 kg/(m^2 s)) thus validating the nearly constant mass flow rate assumption.

3.2. Influence of pressure and temperature

Table 3 shows the density and viscosity values for the liquid and fluid phase used in the simulations at all the studied temperature and pressure conditions. Table 4 shows the calculated IPA diffusion coefficients and mass transfer coefficients in the liquid and fluid phases. Note that, due to the hypothesis of constant fluid properties along the column, single values of k_L and k_F are calculated for each condition.

Fig. 4 shows numerical and experimental results of IPA mass fraction and recovery ratio of water and IPA in the raffinate phase as a function of operating pressure, at constant temperature (40 °C) and Q_F/Q_L ratio (6.04 kg/kg), for the fractionation of a 5% IPA solution using springs packing. Experimental results are given in terms of composition and recovery ratio in raffinate, because, on an experimental point of view, this outlet phase is easier to recover and analyse than the extract phase. Recovery ratio in the raffinate is obtained by dividing the flowrate of the considered compound in the raffinate by the flowrate of the compound in the feed.

The experimental reproducibility has been assessed and demonstrated in our previous work [18]. Each run was reproduced in quadruplicate and results were found reproducible with a mean deviation equal to 0.005% for raffinate IPA mass fraction and 0.35% for raffinate

Table 2
Packed column parameters used in the calculations.

Parameter	Value
Column length (m)	2
Column internal diameter (m)	0.0175
Packing dry void fraction	0.75 (springs) 0.92 (foam)
Packing characteristic length (m)	0.003 (springs) 0.004 (foam)
Packing specific surface area (m^2/m^3)	942 (springs) 610 (foam)
Stainless steel “critical” surface tension (N/m)	0.075

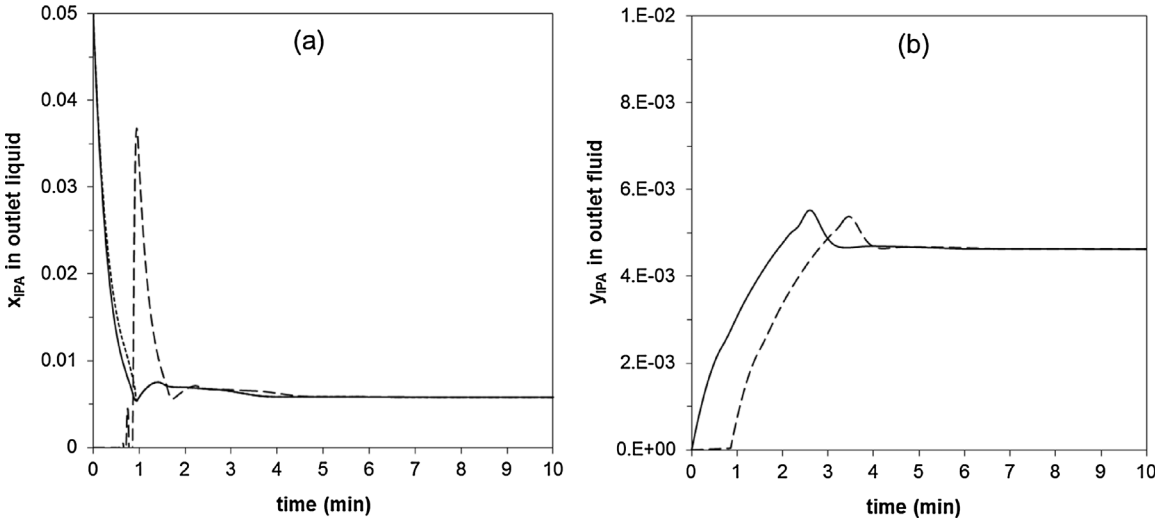

Fig. 2. IPA concentration in liquid (a) and fluid (b) outlet currents vs. time for the fractionation of a 5% IPA solution at T = 40 °C, P = 10 MPa, Q_L = 0.48 kg/h and Q_F/Q_L = 9.5 kg/kg, using different initial liquid phase profiles: (- -) pure water; (—) 5% IPA solution; (···) linear profile.

IPA recovery ratio.

The values of the coefficients of the Onda correlations (α and β) were manually fitted in order to reproduce the experimental results, with a good agreement using $\alpha = 1.05$ and $\beta = 0.001$, valid for all experiments related to the springs packing at 40 °C. With these values, the absolute average relative deviation (AARD) was 16.4% for the IPA mass fraction and 17.6% for the IPA recovery, both in the raffinate. This implies that the mass transfer coefficient values predicted by the original correlations of Onda are divided approximately by 5 in order to reproduce the experimental data obtained in our column. Onda's correlations were developed from data obtained in conventional gas-liquid systems, at atmospheric pressure, and therefore may not be directly applicable to our specific case, in which the gas phase is replaced by a dense supercritical phase and the packing type and column dimensions may induce specific flow patterns. Therefore, the original coefficients were replaced by adjustable parameters in order to account for these features. Concerning flow patterns, it must be remembered that the correlations of Onda were developed from data obtained in gas absorption packed columns with a high ratio between column diameter and packing size. In our fractionation column, this ratio is lower and

Table 3
Fluid and liquid phase properties used in the calculations.

T (°C)	P (MPa)	ρ_F (kg/m^3)	$\mu_F \times 10^5$ (Pa s)	ρ_L (kg/m^3)	$\mu_L \times 10^4$ (Pa s)
40	10	630	5.00	996	6.54
40	12	718	5.85	997	6.54
40	15	780	6.75	999	6.54
40	20	840	7.83	1001	6.55
50	10	384	2.84	992	5.49
60	10	290	2.38	987	4.69
70	10	248	2.25	982	4.06
80	10	222	2.20	976	3.57

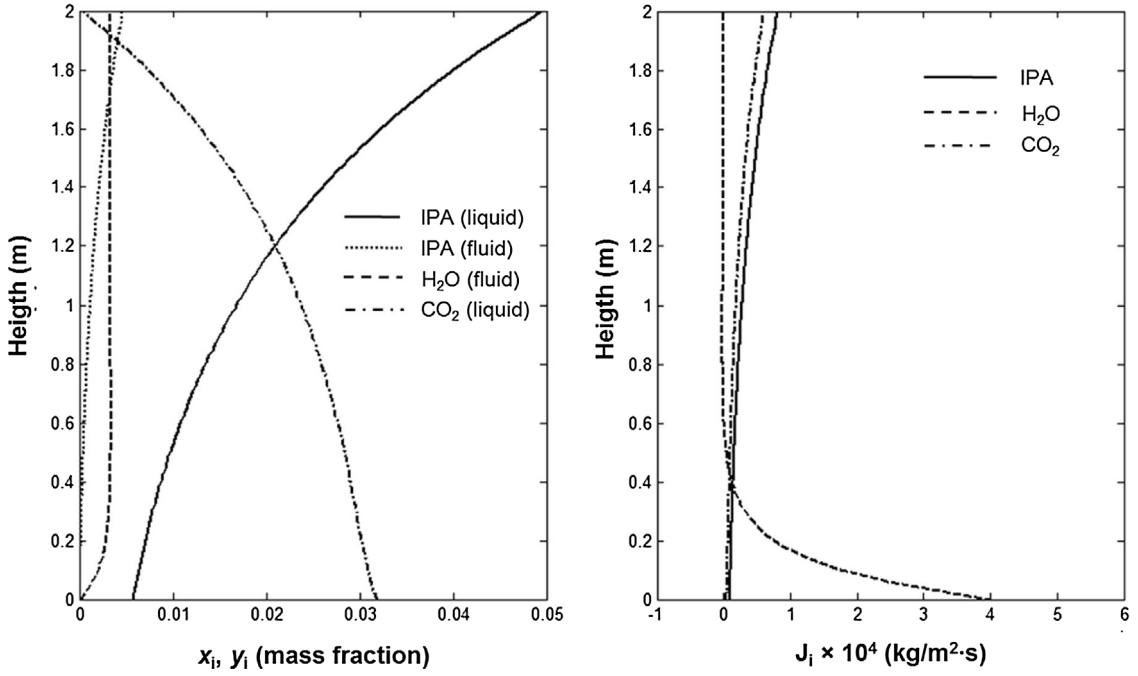

Fig. 3. Calculated mass fraction of compounds (x_i, y_i) and mass transfer flux (J_i) profiles for the fractionation of a 5% IPA solution at T = 40 °C, P = 10 MPa, Q_L = 0.48 kg/h and Q_F/Q_L = 9.5 kg/kg using springs packing. The calculation time was 10 min, corresponding to the steady state solution.

Table 4
Calculated IPA diffusion coefficient (D) and mass transfer coefficient (k) in fluid and liquid phase.

T (°C)	P (MPa)	$D_F \times 10^8$ (m^2/s)	$D_L \times 10^9$ (m^2/s)	$k_F \times 10^5$ (m/s)	$k_L \times 10^6$ (m/s)
40	10	2.27	1.79	8.74	2.27
40	12	1.94	1.79	7.11	2.27
40	15	1.68	1.79	5.97	2.27
40	20	1.45	1.79	4.99	2.27
50	10	4.12	2.20	25.92	2.88
60	10	5.07	2.51	34.87	3.34
70	10	5.52	3.16	39.70	4.38
80	10	5.81	3.69	42.98	5.24

wall effects are suspected to be much more pronounced, reducing the effective interfacial area and the column performance. Moreover, axial dispersion has not been taken into account in the model. Thus, it has been chosen to reflect these phenomena, including pressure effects, in the values of mass transfer coefficients.

In Fig. 4, it can be observed that the model describes correctly the enhancing effect of pressure on the column efficiency within the studied range. Although the fluid phase density and viscosity increase with pressure (see Table 3), with a subsequent decrease of the mass transfer coefficient, this effect is compensated by an IPA partition coefficient (m_1) enhancement (almost 2-fold) as CO_2 density increases. This can be seen in Fig. 5, which shows the representative values of m_1 as well as the IPA mass transfer resistance in both phases, defined according to Eqs. (13) and (14):

$$R_{1,F} = \frac{1}{k_{1,F} m_1} \tag{13}$$

$$R_{1,L} = \frac{1}{k_{1,L}} \tag{14}$$

The m_1 values shown in Fig. 5 are mean values calculated for comparison using the column global composition. Although the partition coefficient is composition dependent, in the case of dilute mixtures its variation is limited within a narrow range, as can be seen for a typical run in Fig. 6.

As can be observed in Table 4, the k_L values calculated by the model are practically independent of pressure, because the change in the liquid relevant properties (density and viscosity) with pressure is very low. Therefore, the mass transfer resistance on the liquid side also remains almost constant, as shown in Fig. 5. On the other hand, the k_F

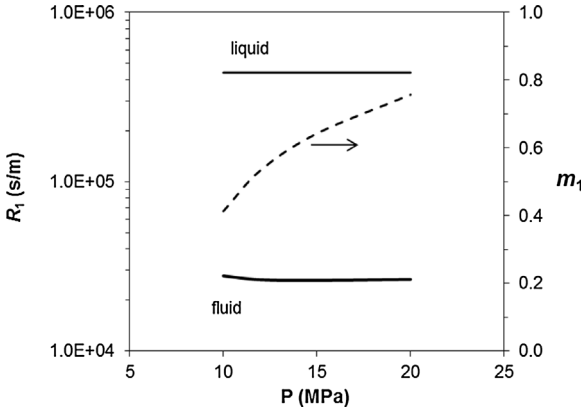

Fig. 5. Calculated IPA partition coefficient (dotted line) and mass transfer resistances (solid lines). Column average values as a function of operation pressure for the fractionation of dilute IPA solutions (5 wt%, T = 40 °C, Q_L = 0.48 kg/h, Q_F/Q_L = 6.04 kg/kg) using springs packing.

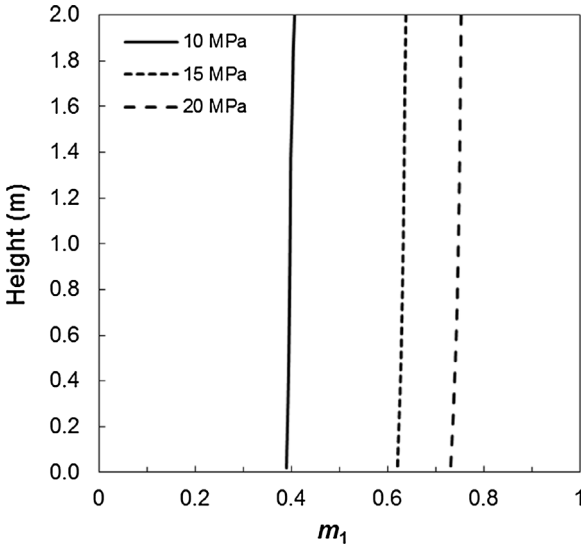

Fig. 6. IPA partition coefficient profile along the column as a function of operation pressure for the fractionation of a 5% IPA solution at T = 40 °C and Q_F/Q_L = 9.5 kg/kg using springs packing.

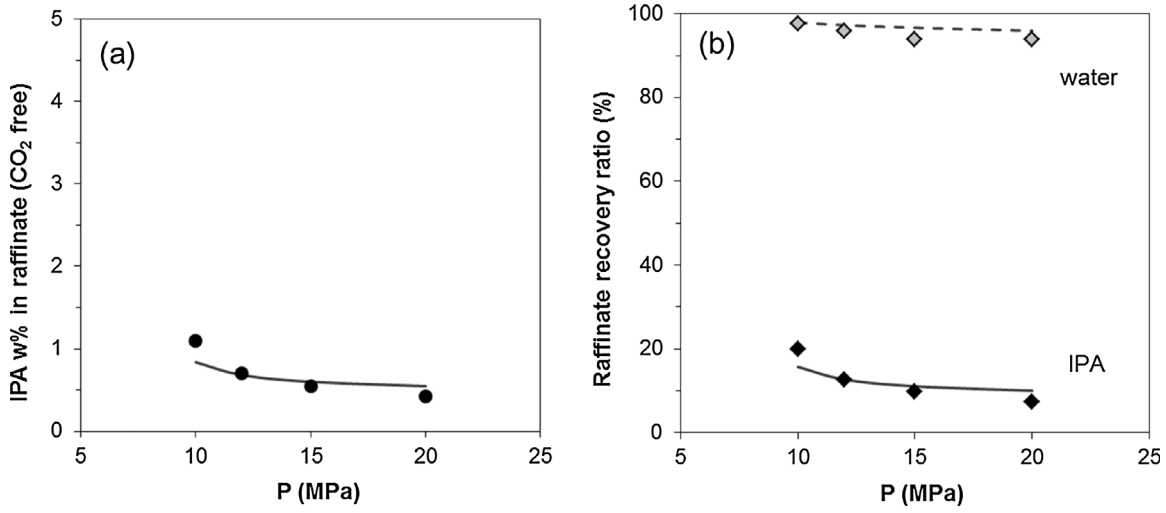

Fig. 4. (a) IPA wt% in raffinate (in CO_2-free basis) and (b) raffinate recovery ratio of IPA and water versus operation pressure for the fractionation of dilute IPA solutions (5 wt%, T = 40 °C, Q_L = 0.48 kg/h, Q_F/Q_L = 6.04 kg/kg) using springs packing. Dots: experimental results from Lalam et al. [18]. Lines: simulation results with α = 1.05 and β = 0.001.

values are more sensitive and decrease with pressure, as the fluid density and viscosity increase. However, due to the combination of this effect with the partition coefficient enhancement, the mass transfer resistance on the fluid phase also remains practically constant. It can also be noticed that the calculated mass transfer resistance on the liquid side is about one order of magnitude higher than on the fluid side. It was reported that the limiting mass transfer resistance in supercritical fluid-liquid operation can be located on the fluid side [37]. However this corresponds to the case of very low solute partition coefficient, as in the case of many high molecular weight lipid compounds. For instance, the partition coefficient of compounds such as squalene, oleic acid, triolein and α-tocopherol in $scCO_2$/oil mixtures range from 0.01 to 0.04 (at 40–60 °C and 10–20 MPa), as reported by several authors [38–40]. In our case, the relatively high IPA partition coefficient values (which are in the range of 0.3–0.8 at the studied operation conditions) explains that the limiting resistance is located on the liquid phase. This is a useful information which indicates that technological improvement of the contactor should focus on increased liquid side mass transfer coefficients in the case of this IPA/water fractionation with $scCO_2$.

The influence of operation temperature on the fractionation performance can be seen in Fig. 7, where experimental and numerical results of IPA concentration and recovery in the raffinate at constant pressure (10 MPa) and solvent-to-feed ratio (9.5 kg/kg) are presented, for the fractionation of a 5% IPA solution using springs packing.

Experimental values indicate that the column efficiency decreases with temperature up to 60 °C. Lalam et al. [18] related this behaviour to the evolution of the IPA partition coefficient, which also decreases from 40 to 60 °C. The authors also predicted, using an equilibrium-stage modeling, that this behaviour reverses above 60 °C. In the present study, simulations, although performed using the previously fitted coefficient at $T = 40$ °C ($\alpha = 1.05$ and $\beta = 0.001$), provided a qualitatively correct description of this trend. However, the simulation results overestimated the separation performance, predicting lower IPA concentration in the raffinate than in the experiments. As shown in Fig. 7, a better agreement could be obtained using different values of α (0.68 at 50 °C and 0.58 at 60 °C) and β ($6.6 \times 10 - 4$ at 50 °C and $5.6 \times 10 - 4$ at 60 °C). In this case, the AARD values were only 3.5% for IPA concentration and 3.2% for IPA recovery. The decreasing values of α and β with temperature are in some way consistent with the original formulation by Onda et al., which considers an inverse relationship between k_F and RT (perfect gas hypothesis) which can be lumped into the coefficient value, becoming T-dependent.

The predicted results are a consequence of the predominant effect of temperature on CO_2 density and solvent power (below 60 °C) and on IPA and water vapour pressure (above 60 °C). This result is consistent with computed IPA partition coefficient in the ternary system at 10 MPa as shown in Fig. 8. Despite its remaining imprecision the thermodynamic model has been found to correctly predict influence of temperature, more particularly on IPA-CO_2 binary system, for which a liquid-vapour equilibrium zone can be observed, both experimentally and with modeling, at temperature above 58 °C at 10 MPa, making the ternary system to switch from Type I to Type II [18]. This behaviour can explain occurrence of the minimum of IPA partition coefficient, shown in Fig. 8 along with the computed correlative mass transfer resistance on the fluid phase side, calculated using constant and variable values for the parameters α and β.

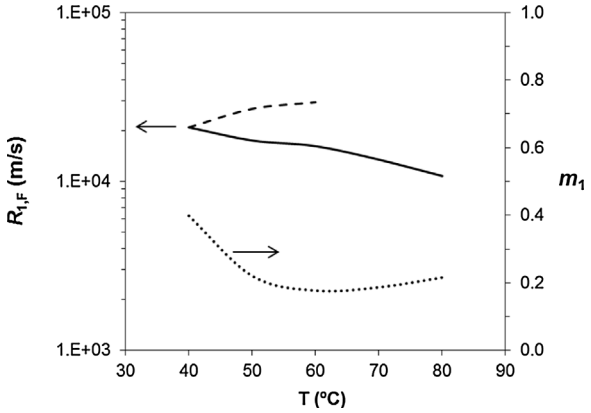

Fig. 8. Calculated IPA partition coefficient (m_1) and fluid phase mass transfer resistance ($R_{1,F}$) as a function of operation temperature for the fractionation of dilute IPA solutions (5 wt%, $P = 10$ MPa, $Q_L = 0.48$ kg/h, $Q_F/Q_L = 9.5$ kg/kg) using springs packing. (···) IPA partition coefficient; (—) fluid phase resistance using $\alpha = 1.05$ and $\beta = 0.001$; (- -) fluid phase resistance using variable α and β values.

3.3. Influence of solvent-to-feed ratio

Fig. 9 shows the numerical simulation results together with the experimental data for the fractionation of a 5% wt. IPA liquid feed at 40 °C and 10 MPa, for different solvent-to-feed (Q_F/Q_L) ratios, using springs packing. These simulations were performed with a constant liquid flow rate (0.48 kg/h) and varying CO_2 flow rate, in the same way as in the experiments. The mass transfer coefficients were calculated using the same coefficients previously adapted at 40 °C and 10 MPa ($\alpha = 1.05$ and $\beta = 0.001$).

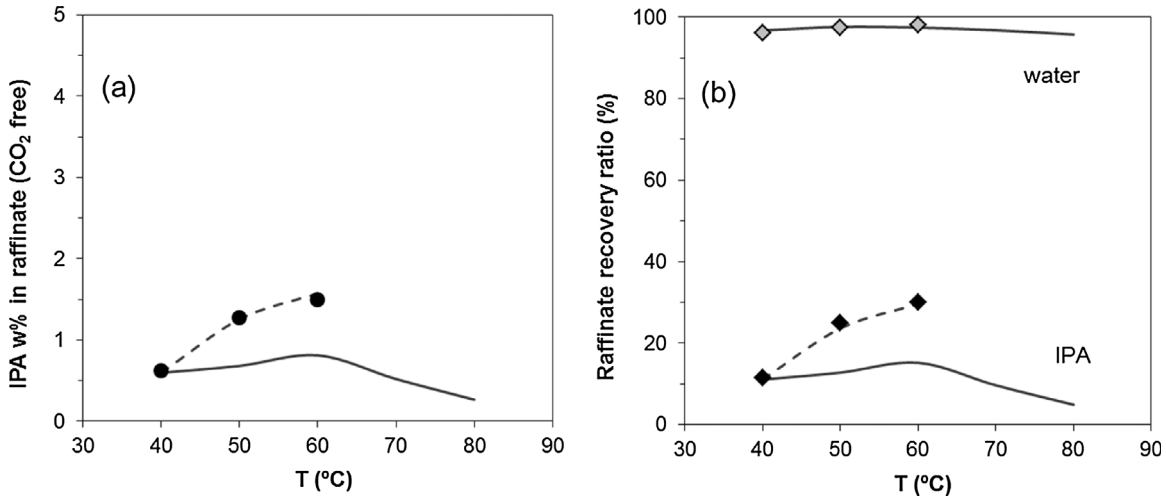

Fig. 7. (a) IPA wt% in raffinate (in CO_2-free basis) and (b) raffinate recovery ratio of IPA and water versus operation temperature for the fractionation of dilute IPA solutions (5 wt%, $P = 10$ MPa, $Q_L = 0.48$ kg/h, $Q_F/Q_L = 9.5$ kg/kg) using springs packing. Dots: experimental results from Lalam et al. [18]. Solid lines: simulation results with $\alpha = 1.05$ and $\beta = 0.001$. Dotted lines: simulation results using variable α and β values.

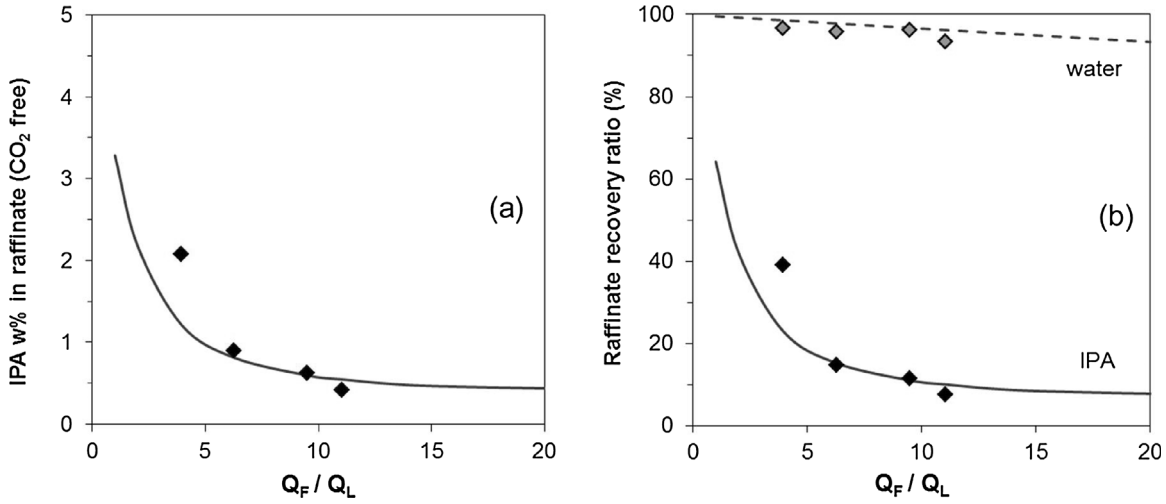

Fig. 9. (a) IPA wt% in raffinate (in CO_2-free basis) and (b) raffinate recovery ratio of IPA and water versus solvent-to-feed ratio for the fractionation of dilute IPA solutions (5 wt%, T = 40 °C, P = 10 MPa, Q_L = 0.48 kg/h) using springs packing. Dots: experimental results from Lalam et al. [18]. Lines: simulation results with α = 1.05 and β = 0.001.

It can be seen that the model was able to fairly reproduce the experimental data trend (AARD of 21.3% and 20.6% for IPA concentration and recovery, respectively), with a good matching for $Q_F/Q_L \geq 6$ but higher deviations at $Q_F/Q_L < 6$. In fact, for low Q_F/Q_L ratios (< 6) the model overpredicts the fractionation performance, yielding to lower concentration values of IPA in the raffinate phase than those observed experimentally. In this low Q_F/Q_L region, lower values of the parameters α and β should be used in order to reproduce correctly the experimental results, as discussed in the next paragraph. This possibly indicates a change in the column hydrodynamic regime, which is not explicitly taken into account in the applied correlations. In particular, as low Q_F/Q_L ratio correspond to low CO_2 flow rate, a hypothesis could be that the column is operated at conditions below loading point, where liquid and CO_2 phases weakly interact.

Simulations were also performed at higher Q_F/Q_L ratios (up to 20), predicting that for $Q_F/Q_L > 15$ the recovery and concentration of IPA in the raffinate change at a very low rate. Operation in this region becomes more expensive, as the cost of CO_2 recompression increases, with only a minor improvement in the separation efficiency. Besides, it can be observed from raffinate recovery ratio (Fig. 9(b)) that the extraction of water in the supercritical fluid phase increases, reducing selectivity of extraction and thus the IPA purity in the extract.

3.4. Influence of packing type

In order to evaluate the model performance with different packing characteristics, simulations were performed and compared with experimental results using a metallic foam packing, as reported by Lalam et al. The main characteristics of this foam are presented in Table 2.

Fig. 10 shows the experimental and numerical results for the fractionation of a 5% IPA solution at 10 MPa and 40 °C and at different Q_F/Q_L ratios. The results with springs packing are also presented for comparison. Numerical results for the foam packing were calculated using α = 1.38 and β = 0.0018 as adjusted coefficients. As in the case of springs, a fair agreement was obtained for $Q_F/Q_L > 6$ (AARD of 33% for IPA concentration and recovery in the raffinate), with higher deviations for $Q_F/Q_L < 6$ (47%).

It is interesting to note that, for both types of packing, there seems to be a change in the experimental data slope around Q_F/Q_L = 6, which is not correctly reproduced by the model. As mentioned, this may be due to a change in the column hydrodynamic regime and inner flow patterns, which would affect the phase distribution, the effective interfacial area as well as the mass transfer coefficient values. This sudden change of behaviour can also remind the conventional “loading point” of a packed bed as encountered in gas-liquid columns. This analogy

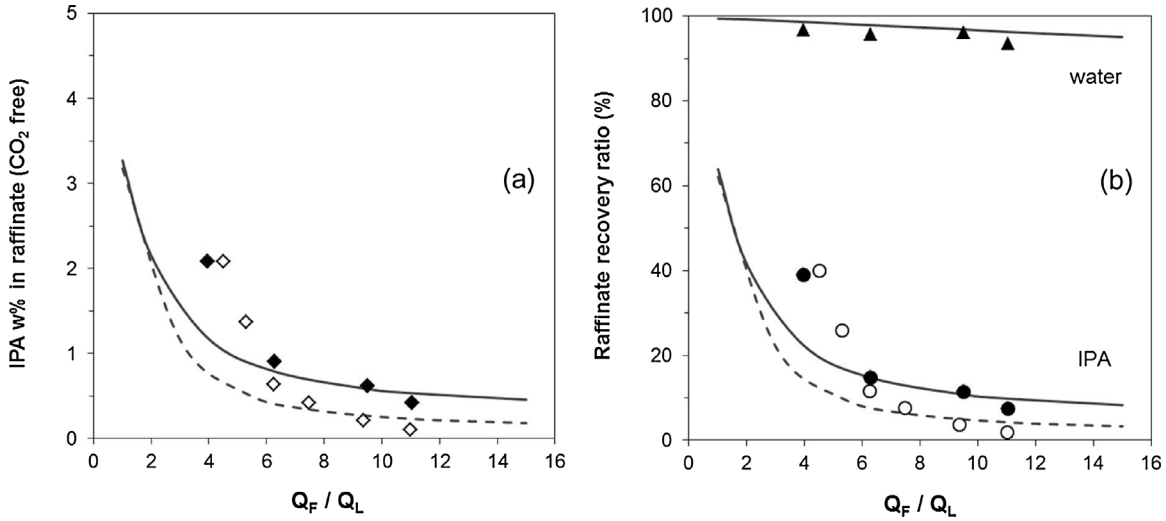

Fig. 10. (a) Raffinate recovery ratio of IPA and water and (b) IPA wt% in raffinate (in CO_2-free basis) versus solvent-to-feed ratio for the fractionation of dilute IPA solutions (5 wt%, T = 40 °C, P = 10 MPa, Q_L = 0.48 kg/h) using stainless steel springs (solid lines and black dots) and metallic foam packing (dotted lines and empty dots).

could be envisaged as an explanation, as experiments have been done far below the flooding point (visually observed at the top of the column). Another hypothesis could be a change in nature of the continuous phase, which is assumed in our case to be CO_2 phase, whatever operating conditions.

Fig. 11 shows the calculated IPA mass transfer resistances for the liquid and fluid phase, along with the mean IPA partition coefficient, as a function of the Q_F/Q_L ratio, for both packing types. It can be seen that the resistance in both phases is somewhat lower in the case of the metallic foam packing, which is consistent with the slightly better separation performance observed experimentally. On a mass transfer point of view, this result could be surprising, considering the specific surface of foam which is given to be equal to 610 m^2/m^3, i.e., significantly lower than 1184 m^2/m^3, the estimated spring packing specific area. Indeed, the appropriate parameter is the "effective" interfacial area (in our case supposed to be equal to the wetted surface) rather than the geometrical packing area and experimental results would indicate that effective interfacial area is greater in the case of foam as compared to springs. It is important to mention that the geometrical surface area of the springs packing has been calculated considering the entire surface of the wire constituting the spring. Therefore the wetted surface, computed from this value using the Onda's correlation, is very probably largely overestimated. Moreover, it is expected that due to the specific shape of foam, wall effect should be reduced and distribution of the liquid should be improved, leading to weaker wall effects and ultimately to a higher effective surface area than in the case of spring packing. Because of global better mass transfer performances for the foam packing, the corresponding values of α and β have been found to be higher than for the springs packing.

4. Conclusions

In this work, a dynamic rate-based numerical model was developed to allow fast computation of counter-current fractionation of dilute liquid mixtures with $scCO_2$ in packed columns. The model is based on a set of differential mass balance equations and algebraic equations (assuming plug flow for the two phases) and correlations that take into account thermodynamics and mass transfer phenomena. The mass transfer model is based on the "double resistance" approach, assuming phase equilibrium at the interface and calculating the mass transfer fluxes using local mass transfer coefficients.

The model was validated by comparison with experimental data obtained in a bench-scale isothermal column for processing of dilute aqueous solutions of IPA with $scCO_2$. The physicochemical properties of the pure compounds and mixtures were taken from literature (if available) or estimated with reliable numerical methods. Ternary phase equilibrium was computed using the thermodynamic software Simulis© Thermodynamics.

Simulations were performed at different temperature, pressure and solvent-to-feed ratios, and with two types of packing (stainless steel springs and a metallic foam), with different geometrical properties. Using two adjustable coefficients included in the equations for the mass transfer coefficients in both phases, a good agreement could be achieved between the experimental and calculated results. The effects of pressure and temperature on IPA concentration and recovery in the raffinate were satisfactorily reproduced and explained in terms of the properties of the phases and the solute partition coefficient. The effect of solvent flow rate could be well described at values $Q_F/Q_L > 6$, but higher deviations were observed at lower solvent-to-feed ratios.

In addition to provide a tool for optimizing the operation conditions, the model also allows to compare the mass transfer resistance in both phases, indicating that, in our case, the main resistance was located on the liquid side. This was connected with the enhanced transport properties of the supercritical fluid as well as with the relatively high partition coefficient of IPA.

Such a model is an attempt to develop a realistic and convenient modeling tool, more easily generalizable than theoretical stage based modeling as shown in previous work [18]. Nevertheless, its relative simplicity was obtained at the expense of its range of validity because it involves the hypothesis of constant flow rates and is therefore restricted to the processing of dilute mixtures. Also, its predictability is handicapped by the need to adjust some coefficients for the computation of the local mass transfer coefficients. Nevertheless, we believe that it can be helpful to interpret experimental data in order to optimize operating conditions or be a guidance towards technological improvement of the contactor.

Acknowledgements

N.A. Gañán acknowledges CONICET (Argentina) for his post-doctoral fellowship, as well as Erasmus Mundus – Lamenitec Program for his mobility scholarship at INSA-Toulouse (France).

Appendix A. Method of Tamura.

This method allows the estimation of the surface tension of aqueous mixtures of organic solutes by interpolation of the surface tension of the pure compounds at the same temperature.

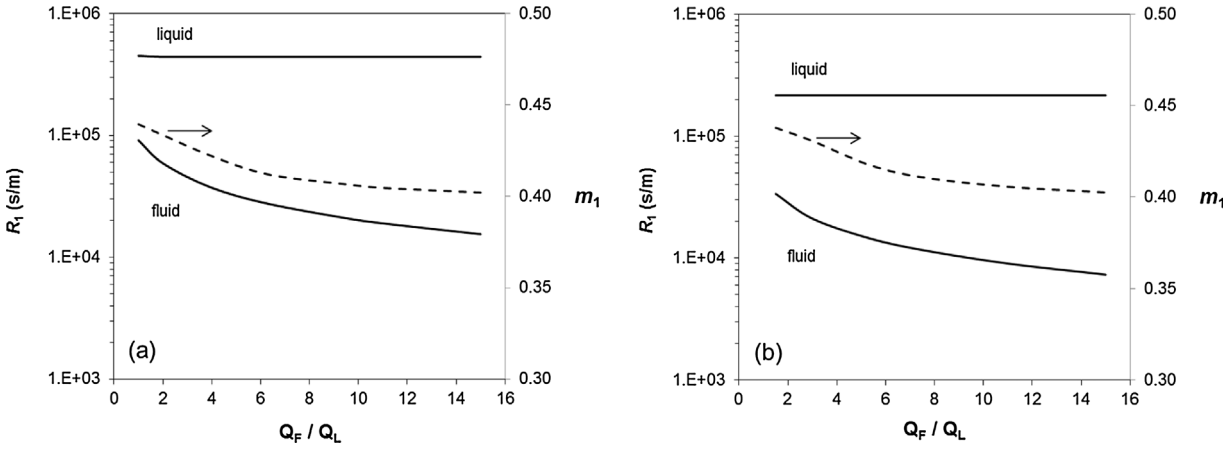

Fig. 11. Calculated IPA partition coefficient (dotted line) and mass transfer resistance in each phase (solid lines). Column average values versus solvent-to-feed ratio for the fractionation of dilute IPA solutions (5 wt%, T = 40 °C, P = 10 MPa, Q_L = 0.48 kg/h) using (a) springs, and (b) metallic foam packing.

The basic equation is:

$$\sigma_m^{1/4} = \psi_w^{\sigma} \sigma_w^{1/4} + \psi_o^{\sigma} \sigma_o^{1/4} \tag{A.1}$$

where σ_m is the mixture surface tension, σ_w and σ_o are the surface tension of pure water and the pure organic solute (at the same temperature), and Ψ^{σ}_w, Ψ^{σ}_o are the superficial volume fractions of water and solute in the surface layer. The model consists in the following set of equations:

$$B = \log \frac{(\psi_w)^q}{\psi_o} \tag{A.2}$$

$$W = 0.441 \frac{q}{T} \left(\frac{\sigma_o V_o^{2/3}}{q} - \sigma_w V_w^{2/3} \right) \tag{A.3}$$

$$\frac{(\psi_w^{\sigma})^q}{\psi_o^{\sigma}} = 10^{(B+W)} \tag{A.4}$$

where V_w, V_o are the molar volumes of pure water and the pure organic solute, T is the absolute temperature, q is a parameter which depends on the type and size of the organic solute (for alcohols, it is equal to the number of carbon atoms in the molecule), and Ψ_w, Ψ_o are the superficial bulk volume fractions of water and organic solute, defined as:

$$\psi_w = \frac{x_w V_w}{x_w V_w + x_o V_o} \tag{A.5}$$

$$\psi_o = \frac{x_o V_o}{x_w V_w + x_o V_o} \tag{A.6}$$

This set of equations can be solved provided the values of V_w, V_o, x_w, x_o, σ_w, σ_o, q and T, considering that:

$$\psi_w^{\sigma} + \psi_o^{\sigma} = 1 \tag{A.7}$$

In this work, in order to take into account the effect of $scCO_2$, the surface tension of pure water (σ_w) was replaced by the value for water under CO_2 pressure within the experimental range covered here. More details can be found in the work by Tamura et al. [41].

Appendix B. Method of Wilke and Chang.

This method provides an estimation of the diffusion coefficient of a solute (A) in a solvent (B) at infinite dilution conditions (D^o_{AB}). The equation is:

$$D^o_{AB} = \frac{7.4 \times 10^{-8} (\phi M_B)^{1/2} T}{\mu_B V_A^{0.6}} \tag{B.1}$$

where M_B and μ_B are the solvent molar mass (g/mol) and viscosity (cP), V_A is the molar volume of the solute at its normal boiling temperature (cm^3/mol), T is the system temperature (K) and ϕ is the association factor of the solvent (ranging from 2.6 if the solvent is water to 1.0 if it is unassociated).

References

[1] G. Brunner, Counter-current separations (Review), J. Supercrit. Fluids 47 (2009) 574–582.
[2] A. Bejarano, P.C. Simoes, J.M. del Valle, Fractionation technologies for liquid mixtures using dense carbon dioxide, J. Supercrit. Fluids 107 (2016) 321–348.
[3] E. Reverchon, A. Marciano, M. Poletto, Fractionation of a peel oil key mixture by supercritical CO_2 in a continuous tower, Ind. Eng. Chem. Res. 36 (1997) 4940–4948.
[4] M. Sato, M. Kondo, M. Goto, A. Kodama, T. Hirose, Fractionation of citrus oil by supercritical countercurrent extractor with side-stream withdrawal, J. Supercrit. Fluids 13 (1998) 311–317.
[5] M. Budich, S. Heilig, T. Wesse, V. Leibküchler, G. Brunner, Countercurrent deterpenation of citrus oils with supercritical CO_2, J. Supercrit. Fluids 14 (1999) 104–114.
[6] S. Díaz, S. Espinosa, E.A. Brignole, Citrus peel oil deterpenation with supercritical fluids. Optimal process and solvent cycle design, J. Supercrit. Fluids 35 (2005) 49–61.
[7] S. Espinosa, S.B. Bottini, E.A. Brignole, Process analysis and phase equilibria for the removal of chemicals from fatty oils using near-critical solvents, Ind. Eng. Chem. Res. 39 (2000) 3024–3033.
[8] V. Riha, G. Brunner, Separation of fish oil ethyl esters with supercritical carbon dioxide, J. Supercrit. Fluids 17 (2000) 55–64.
[9] O.J. Catchpole, J.B. Grey, K.A. Noermark, Fractionation of fish oils using supercritical CO_2 and CO_2+ethanol mixtures, J. Supercrit. Fluids 19 (2000) 25–37.
[10] L. Vázquez, C.F. Torres, T. Fornari, F.J. Señoráns, G. Reglero, Recovery of squalene from vegetable oil sources using countercurrent supercritical carbon dioxide extraction, J. Supercrit. Fluids 40 (2007) 59–66.
[11] T. Fornari, L. Vázquez, C.F. Torres, E. Ibáñez, F.J. Señoráns, G. Reglero, Countercurrent supercritical fluid extracion of different lipid-type materials: experimental and thermodynamic modelling, J. Supercrit. Fluids 45 (2008) 206–212.
[12] E.A. Brignole, P.M. Andersen, A. Fredenslund, Supercritical fluid extraction of alcohols from water, Ind. Eng. Chem. Res. 26 (1987) 254–261.
[13] M. Budich, G. Brunner, Supercritical fluid extraction of ethanol from aqueous solutions, J. Supercrit. Fluids 25 (2003) 45–55.
[14] M.S. Díaz, E.A. Brignole, Modeling and optimization of supercritical fluid processes, J. Supercrit. Fluids 47 (2009) 611–618.
[15] R. Ruivo, A. Paiva, J.P.B. Mota, P. Simões, Dynamic model of a countercurrent packed column operating at high pressure conditions, J. Supercrit. Fluids 32 (2004) 183–192.
[16] J. Fernandes, R. Ruivo, J.P.B. Mota, P. Simoes, Non-isothermal dynamic model of a supercritical fluid extraction packed column, J. Supercrit. Fluids 41 (2007) 20–30.
[17] A. Martín, J.M. Cocero, Mathematical modeling of the fractionation of liquids with supercritical CO_2 in a countercurrent packed column, J. Supercrit. Fluids 39 (2007) 304–314.
[18] R. Lalam, S. Chamali, S. Camy, D. Rouzineau, R. Kessas, J.-S. Condoret, Fractionation of aqueous isopropanol mixtures in a countercurrent packed column using supercritical CO_2, J. Supercrit. Fluids 101 (2015) 24–35.
[19] P.J. Rathkamp, J.L. Bravo, J.R. Fair, Evaluation of packed columns in supercritical extraction processes, Solvent Extr. Ion Exch. 5 (1987) 367–391.
[20] K. Onda, H. Takeuchi, Y. Okumoto, Mass transfer coefficients between gas and liquid phases in packed columns, J. Chem. Eng. Jpn. 1 (1968) 56–62.
[21] C.J. King, Separation Processes, 2nd edition, McGraw-Hill, 1980.
[22] P.C. Simões, H.M. Matos, P.J. Carmelo, E. Gomes de Azevedo, M. Nunes da Ponte, Mass transfer in countercurrent packed columns: applications to supercritical CO2 extraction of terpenes, Ind. Eng. Chem. Res. 34 (1995) 613–618.
[23] R. Stockfleth, G. Brunner, Hydrodynamics of a packed contercurrent column for the gas extraction, Ind. Eng. Chem. Res. 38 (1999) 4000–4006.
[24] G.F. Woerlee, Hydrodynamics and Mass Transfer in Packed Columns and Their Applications for Supercritical Separations, Delft University Press, Delft, 1997 PhD Thesis.
[25] T. Otake, K. Okada, Liquid hold-up in packed towers, operating and hold-up without gas flow, Kagaku Kogaku (Japanese) 17 (1953) 176–184.
[26] G. Soave, Equilibrium constants from a modified Redlich–Kwong equation of state, Chem. Eng. Sci. 27 (1972) 1197–1203.
[27] J.F. Boston, P.M. Mathias, Phase equilibria in a third-generation process simulator, Proceedings of the 2nd International Conference on Phase Equilibria and Fluid

Properties in the Chemical Process Industries, West Berlin, 1980, pp. 823–849.
[28] T. Holderbaum, J. Gmehling, PSRK: a group contribution equation of state based on UNIFAC, Fluid Phase Equilib. 70 (1991) 251–265.
[29] D.S. Abrams, J.M. Prausnitz, Statistical thermodynamics of liquid mixture: a new expression for the excess Gibbs energy of partly or complete miscible systems, AIChE J. 21 (1975) 116–128.
[30] T.F. Anderson, J.M. Prausnitz, Application of the UNIQUAC equation to calculation of multi-component phase equilibria: 1. Vapor–liquid equilibria, Ind. Eng. Chem. Proc. Des. Dev. 17 (1978) 552–560.
[31] A. Hebach, A. Oberhof, N. Dahmen, Density of water + carbon dioxide at elevated pressures: measurements and correlation, J. Chem. Eng. Data 49 (2004) 950–953.
[32] I. Tsivintzelis, D. Missopolinou, K. Kalogiannis, C. Panayiotou, Phase compositions and saturated densities for the binary systems of carbon dioxide with ethanol and dichloromethane, Fluid Phase Equilib. 224 (2004) 89–96.
[33] B.E. Poling, J.M. Prausnitz, J.P. O'Connell, The Properties of Gases and Liquids, 5th edition, McGraw-Hill, 2001.
[34] Y. Tanaka, Y. Matsuda, H. Fujiwara, H. Kubota, T. Makita, Viscosity of (water + alcohol) mixtures under high pressure, Int. J. Thermophys. 8 (1987) 147–163.
[35] G. Brunner, Gas Extraction: An Introduction to Fundamentals of Supercritical Fluids and the Application to Separation Processes, Topics in Physical Chemistry vol. 4, Steinkopff; Springer, Darmstadt; New York, 1994.
[36] B.-S. Chun, G.T. Wilkinson, Interfacial tension in high-pressure carbon dioxide mixtures, Ind. Eng. Chem. Res. 34 (1995) 4371–4377.
[37] R. Ruivo, M.J. Cebola, P.C. Simoes, M. Nunes da Ponte, Fractionation of edible oil model mixtures by supercritical carbon dioxide in a packed column. 2. A mass-transfer study, Ind. Eng. Chem. Res. 41 (2002) 2305–2315.
[38] T. Fang, M. Goto, Z. Yun, X. Ding, T. Hirose, Phase equilibria for binary systems of methyl oleate–supercritical CO_2 and α-tocopherol–supercritical CO_2, J. Supercrit. Fluids 30 (2004) 1–16.
[39] R. Bharath, H. Inomata, T. Adschiri, K. Arai, Phase equilibrium study for the separation and fractionation of fatty oil components using supercritical carbon dioxide, Fluid Phase Equilib. 81 (1992) 307–320.
[40] O.J. Catchpole, J.B. Grey, K.A. Noermark, Solubility of fish oil components in supercritical CO_2 and CO_2 + ethanol mixtures, J. Chem. Eng. Data 43 (1998) 1091–1095.
[41] M. Tamura, M. Kurata, H. Odani, Practical method for estimating surface tensions of solutions, Bull. Chem. Soc. Jpn. 28 (1955) 83–88.